Electrochemical immunosensors using electrodeposited gold nanostructures for detecting the S proteins from SARS-CoV and SARS-CoV-2

Laís Canniatti Brazaca[1,2*], Amanda Hikari Imamura[1,2], Nathalia Oezau Gomes[1], Mariana Bortholazzi Almeida[1,2], Desirée Tamara Scheidt[1,2], Paulo A. Raymundo-Pereira[3], Osvaldo N. Oliveira Jr[3], Bruno Campos Janegitz[4], Sergio Antonio Spinola Machado[1], Emanuel Carrilho[1,2*]

1) Instituto de Química de São Carlos, Universidade de São Paulo, São Carlos, SP, 13566-590, Brazil

2) Instituto Nacional de Ciência e Tecnologia de Bioanalítica-INCTBio, Campinas, SP, 13083-970, Brazil

3) Instituto de Física de São Carlos, Universidade de São Paulo, São Carlos, SP, 13566-590, Brazil

4) Departamento de Ciências da Natureza, Matemática e Educação, Universidade Federal de São Carlos, Araras, SP, 13600-970, Brazil.

*Corresponding Authors:

Laís Canniatti Brazaca (Ph.D.) Email: lais.brazaca@usp.br

Current Address: Bioanalysis, Microfluidics and Separations Group, University of São Paulo, São Carlos Institute of Chemistry – 400, Trabalhador São-carlense avenue, CEP 13566-590, São Carlos, SP, Brazil

Telephone Number: +55 16 3373 8279

E.C.: emanuel@iqsc.usp.br

Abstract

This paper reports a sensitive strategy for fast determination of S proteins from both SARS-CoV and SARS-CoV-2 using a single disposable, low-cost (<US$ 0.03 per device) immunosensor made with modified screen-printed carbon electrodes (SPCEs). Gold nanoparticles were electrochemically deposited via direct reduction of gold ions on the electrode using amperometry. Capture antibodies from spike (S) protein were covalently immobilized on carboxylic groups of self-assembled monolayers (SAM) of mercaptoacetic acid (MAA) attached to the gold nanoparticles. Label-free detection of S proteins from both SARS-CoV and SARS-CoV-2 was performed with electrochemical impedance spectroscopy (EIS). The immunosensor fabricated with 9 s gold deposition had a high performance in terms of selectivity, sensitivity, and low limit of detection (LOD) (3.39 pmol L^{-1}), thus permitting the direct determination of the target proteins in spiked saliva samples. The complete analysis can be carried out within 35 min using a simple one-step assay protocol with small sample volumes (10 µL). With such features, the immunoplatform presented here can be deployed for mass testing in point-of-care settings.

Keywords: SARS-CoV; SARS-CoV-2; S protein; diagnosis; immunosensor; gold nanoparticles.

1. INTRODUCTION

The crisis with Covid-19 has highlighted the need for analytical devices to monitor and detect high-incident diseases caused by viruses and other pathogens with rapid propagation and mutations. Lowcost, portable analytical sensors [1–3] are perhaps the only alternative for the diagnosis of such infections as the one caused by the coronavirus (SARS-CoV-2) [4, 5]. Indeed, the lack of such sensors explains why developing countries could not test their population to the extent recommended by the World Health Organization, which would have been essential for the monitoring to prevent the person-to-person transmission chain [6, 7]. Mass testing has been almost entirely based on molecular techniques, especially real-time polymerase chain reaction (RT-PCR), which is not amenable to use outside specialized laboratories. At the research level, various methods have been used to diagnose SARS-CoV-2 infection via the detection of S or N proteins in different biological matrices [8–10]. A summary of the sensors developed in recent months is presented in the Supplementary Material (Section S1 and Table S2). The particular relevances of our work are the electrochemical immunoassays. For example, carbon black-based screen printed electrodes (SPE) and magnetic beads (MBs) were used to immobilize antibodies and detect S and N proteins with limits of detection (LOD) of 19 ng mL^{-1} and 8 ng mL^{-1}, respectively [8]. A working electrode (WE) coated with graphene oxide (GO) was modified with 8-hydroxyquinoline (8H), 1-ethyl-3-(3-dimethylamino-propyl)carbodiimide (EDC), and N-hydroxysuccinimide (NHS) coupled with gold nanostars (AuNS), generating an ultrasensitive sensor that could detect the trace of viruses in aquatic biological media [6].

Electrochemical sensors with a set of electrodes, viz. working (WE), reference (RE), and counter (CE) electrodes, allow for multi-target detection, simple arrays,

portability, and fast responses, being ideal for applications *in situ* [2, 11, 12]. Analytes can be detected and quantified through redox reactions when binding occurs between the target and the biorecognition element [13], and, therefore, the sensing performance depends strongly on the WE material [14, 15]. SPEs are suitable for mass production and miniaturization at low prices, being advantageous compared with typical solid electrodes [16–18]. They may be produced on almost any type of substrate, either rigid or flexible, and on stretchable surfaces, using different materials [19], including paper [20], ceramic [21], and polymers [22]. When used in conjunction with nanomaterials, SPEs may lead to highly sensitive electrochemical sensors [2, 23]. In this context, electrodeposited gold on SPEs enhances electrochemical activity [24] owing to a facilitated electron transfer and catalytic activity for oxidation and reduction reactions [2, 23, 25, 26]. Gold deposition as a film ensures high conductivity, large surface-area-to-volume ratios, and enables modification with biomolecules. The properties of the gold layer may be tuned by varying the deposition potential (E_d) and deposition time (t_d), thus permitting the optimization of sensing performance [24, 27, 28].

In this study, we developed an immunosensor that can detect the S proteins of SARS-CoV and SARS-CoV-2 using a gold-carbon composite material. To the best of our knowledge, this is the first time a single biosensor is used to detect both pathogens.

2. MATERIALS AND METHODS

2.1. Chemicals

Hydrogen tetrachloroaurate (III), mercaptoacetic acid (MAA), EDC, NHS, bovine serum albumin (BSA), potassium hexacyanoferrate (II) trihydrate, potassium

hexacyanoferrate (III), fluorescein 5(6)-isothiocyanate (FITC), and sulfuric acid (H_2SO_4) were purchased from Sigma Aldrich (USA). Carbon paste ink (ELETRODAG 423SS E&C) was obtained from LOCTITE® (Germany), and Ag/AgCl ink (90701) was acquired from TICON (Brazil). Anti-SARS-CoV S protein antibodies (40150-D006) and SARS-CoV S protein (40150-V08B2) were purchased from Sino Biological (China), while SARS-CoV-2 glycoprotein S1 (ab273068) was obtained from Abcam (EUA). Polyethylene terephthalate (PET) sheets for electrode fabrication were obtained from local stationery shops and cleaned with isopropyl alcohol before use.

2.2. Fabrication of screen-printed electrodes

The screen-printing technique was used to produce carbon electrodes (Figure 1A). First, a customized polyester screen (77-mesh) (Silk Center, Brazil) was designed using AutoCAD software and produced by Iasa Segmentos Industriais (Brazil). The carbon paste ink was then manually printed on a PET sheet with a polyurethane squeegee. The printed devices containing the three electrodes were then cured at 90 °C for 30 min. The reference electrodes were manually painted with Ag/AgCl ink and dried at 90 °C for 45 min. An insulator adhesive tape was used to delimit the geometric area of the working electrode at 12.56 mm^2.

2.3. Electrodeposition of gold

All electrodes received an electrochemical pretreatment with sulfuric acid (0.5 mol L^{-1}) within a potential range between –2.5 and +2.5 V at a scan rate of 100 mV s^{-1} [29]. Two voltammetry cycles were performed, and the sulfuric acid was completely

replaced after each cycle. Gold nanoparticles were electrogenerated on screen-printed electrodes by applying a constant potential of –4.0 V in an electrochemical cell containing 20 mL 5.0 mmol L^{-1} hydrogen tetrachloroaurate (III) solution with 0.5 mol L^{-1} sulfuric acid under vigorous stirring for 9 s (or 30 s or 90 s) (Figure 1B) [30].

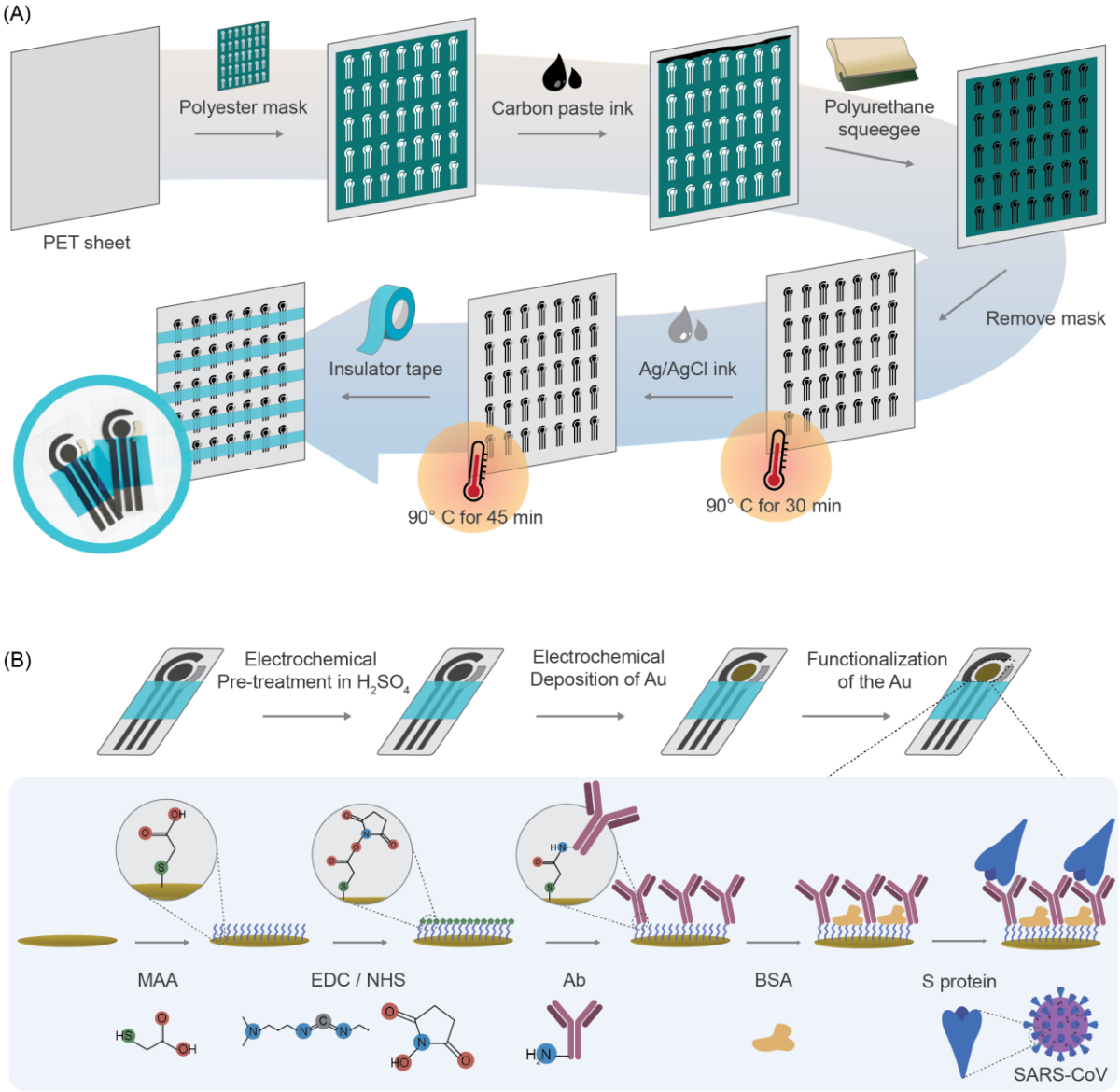

Figure 1. Step-by-step immunosensor fabrication. **(A)** Fabrication steps of the screen-printed electrodes. **(B)** Electrochemical treatments, Au deposition, and modification of working electrodes with antibodies.

2.4. Optical characterization of the modified electrodes

Images of the gold nanostructures were obtained with a scanning electron microscope (SEM) (ZEISS, LE0 440, model 7060) equipped with an OXFORD® system detector. A Thermo Scientific Prisma E Scanning Electron Microscope (SEM) with ColorSEM Technology and integrated energy-dispersive X-ray spectroscopy (EDS) was used to assess the chemical composition of the modified electrodes. The antigen-antibody interaction was studied using a confocal fluorescence microscope Zeiss LSM 780 with an argon laser. SARS-CoV S protein was labeled with fluorescein isothiocyanate (FITC) by mixing the two molecules in a 1:20 ratio for 1 h at room temperature (25 ^{o}C). Dialysis was then used to remove unbound FITC. The fluorescence of the modified electrodes was measured in the absence and presence of labeled S proteins, validating its binding to the biosensor surface.

2.5. Electrochemical characterization of the modified electrodes

Modified electrodes using different gold electrodeposition conditions were characterized using cyclic voltammetry (CV) ~~to assess their analytical properties~~. Bare carbon electrodes and devices submitted to 9, 30, and 90 s of gold deposition protocol were evaluated. First, CV was performed in a potassium hexacyanoferrate (II)/(III) solution (4 mmol L^{-1} each, 0.1 mol L^{-1} PBS, pH 7.0) (2 cycles, 100 mV s^{-1}, from -0.3 to 0.7 V). The electrodes were also submitted to CV in 0.1 mol L^{-1} sulfuric acid to assess the amount of gold present on the electrode (2 cycles, 100 mV s^{-1}, from 0.0 to 1.5 V).

2.6. Functionalization of the gold surface with antibodies

Modified-gold electrodes were pretreated with cyclic voltammetry (CV) (0.0 - 1.5 V, 100 mV s^{-1}, 10 cycles) in sulfuric acid (0.1 mol L^{-1}, ultrapure water). Then, 20 µL of an MAA solution (10 mmol L^{-1}, ultrapure water) was incubated on the gold working electrode. After 2 h, electrodes were washed with ultrapure water and dried using a low N_2 stream. Next, 20 µL of a mixture of EDC and NHS (10 mmol L^{-1} and 20 mmol L^{-1} respectively), MES buffer 100 mmol L^{-1} (pH 6.0) were incubated on the modified electrode for 1 h. The electrodes were then rinsed using MES buffer (100 mmol L^{-1}, pH 6.0) and dried using N_2. 20 µL of a 1 µg mL^{-1} anti-protein S antibodies (PBS, 0.1 mol L^{-1}, pH 7.0) were added to the electrode for 1 h. Electrodes were washed using PBS (0.1 mol L^{-1}, pH 7.0) and dried with an N_2 gas stream. Finally, a BSA solution (1% w/v, 30 min, 0.1 mol L^{-1} PBS, pH 7.0) was incubated on the electrode for 30 min for blocking the bioreceptor layer. After washing the modified electrode with PBS (0.1 mol L^{-1}, pH 7.0) and drying it with N_2, the biosensor was ready for use. The samples were added to the working electrode and incubated for 30 min (0.1 mol L^{-1} PBS, pH 7.0). After this period, electrodes were carefully washed using PBS (0.1 mol L^{-1}, pH 7.0), and electrochemical measurements were performed (Figure 1B). Unless indicated otherwise, positive samples were composed of SARS-CoV S protein, while negative samples were composed of BSA. To reduce the evaporation of the droplets, all the solutions for incubation were performed in a closed container with wet wipes. All procedures were performed at room temperature (25 ^{o}C).

2.7. Electrochemical immunosensing

The charge transfer resistance (R_{ct}) of the immunosensors was determined using electrochemical impedance spectroscopy (EIS) in a potassium hexacyanoferrate (II)/(III) solution (4 mmol L^{-1} each, 0.1 mol L^{-1} PBS, pH 7.0). First, to activate the double layer of the biosensor, a CV was performed (2 cycles, from –0.3 to 0.7 V, 100 mV s^{-1}). Then, EIS measurements were performed in open circuit conditions (OCP) (10 kHz to 100 MHz, E_{ac} 10 mV). The reproducibility of the immunosensor was investigated by analyzing the signal of three parallel assemblies after the interaction with 10^{-9} mol L^{-1} protein S. The variability is quantified in terms of relative standard deviation (RSD) in the signals. Repeatability was assessed using RSD of ten successive measurements in a single immunosensor after interaction with 10^{-9} mol L^{-1} S protein. The limit of detection (LOD) was estimated as the analyte concentration corresponding to an $R_{ct} = b_m + 3s_b$, in which b_m is the mean value for blank samples, and s_b is the standard deviation of the blank measurements (n = 6) [31].

2.8. Biological samples

Real saliva samples were used to test the practical application of the device. A pool of human saliva was obtained from Innovative Research (IRHUSL5ML). The samples were centrifuged at 8,000 rcf for 10 min. Then, the supernatant was spiked with SARS-CoV S protein to reach concentrations from 10^{-11} to 10^{-7} mol L^{-1} or with inactivated SARS-CoV-2 viruses (10^6 PFU mL^{-1}). For the electrochemical analysis of biological samples, SDS 0.05% (w/v in PBS) was used as the washing solution between incubations.

3. RESULTS AND DISCUSSION

3.1. Characterization of Au-modified SPCEs

The photographs of Au-modified SPEs in Figure 2A indicate an increased deposition of Au as the electrodeposition time increases. The chemical composition of the films was confirmed through elemental mapping and EDS measurements in Figure 2B, Figure S1, and Figure S2. While bare SPE has a carbon-based surface, Au features appear with increasing Au deposition. A homogeneous thin film was noted for bare SPE, coated with Au structures with regular size and morphology. Different Au structures are shown in the SEM images of Figure 2C - 2F, with no significant defects for bare SPE and Au-coated SPEs. The bright spots on the images can be attributed to Au, while other features in Figure 2C are graphite flakes and carbon nanoparticles from SPE ink. According to ImageJ processing, the Au nanoparticles increased with electrodeposition time, reaching diameters 143 ± 31, 425 ± 161, and 752 ± 207 nm (n = 10), for 9, 30, and 90 s, respectively. The Au deposition was characterized using cyclic voltammetry in 0.1 mol L^{-1} sulfuric acid. Figure 2G shows no redox peaks for bare SPE (black), as expected. The CVs for SPE/Au are typical of surfaces containing Au in 0.1 mol L^{-1} H_2SO_4, with anodic and cathodic peaks at +1.15 V (E_{pa}) and +0.4 V (E_{pc}) due to oxidation (formation) and reduction of Au oxides, respectively [32]. The concentration of electroactive species (Γ/mol cm^{-2}) of AuNPs on the sensor was estimated with $\Gamma = Q/nFA$, where Q (C) is the background-corrected electric charge calculated by integrating the cathodic peak, n is the number of electrons, F is the

Faraday constant (96,485.34C mol^{-1}), and A is the geometric surface area (0.012 cm^2). The estimated charges (Q) were 111, 392, and 966 μC, and the concentrations of electroactive species were 9.6, 34, and 83 × 10^{-8} mol cm^{-2} for $AuNP_{9s}$, $AuNP_{30s}$, and $AuNP_{90s}$, respectively (Figure S3). The values of Γ increased in the order: $AuNP_{9s}$ < $AuNP_{30s}$ < $AuNP_{90s}$, as expected with the increase in AuNPs with longer deposition times already observed with SEM and EDS. The increase in AuNPs on the electrode leads to an increased reduction peak from Au^+ to Au^0, corroborating the cyclic voltammograms in Figure 2G.

The shape and morphology of the nanoparticles affect the electrochemical properties of modified electrodes, primarily due to the electroactive areas [33, 34]. Thus, the electrodeposition time is a crucial factor, as observed in Figure 2 D-F, with peak current increasing with time due to increased surface area. Thicker films preclude electron transfer and induce a large capacitive current, while the small capacitance prevailing with thin films enhances sensitivity [24]. The importance of patterning SPE with Au structures became apparent in the increased electron transfer compared to bare SPE electrodes, as inferred from CV and EIS measurements. Figure 2H shows the Nyquist diagrams for the four electrodes consisting of semicircles and diffusion straight lines. These were analyzed using a modified Randles equivalent circuit [R_s(CPE[$R_{ct}Z_W$])], where R_s is the solution resistance, R_{ct} is the charge transfer resistance, Z_W is the Warburg impedance, and CPE is a constant phase element. The apparent heterogeneous electron rate constant was determined using k_{app} = $RT/F^2R_{ct}CA$, in which F is the Faraday constant, C is the probe redox concentration in solution (4.0 mmol L^{-1}), R is the gas constant (8.3145 J K^{-1} mol^{-1}), T is the temperature (298 K), A is the geometric area (0.1256 cm^2), and R_{ct} is the charge-transfer resistance obtained by fitting the data. k_{app} values calculated for bare SPE and SPE/Au are listed

in Table S1. R_{ct} for SPE/Au (< 88 Ω) is smaller than for bare SPE (1335 Ω) due to the synergy in having SPE and Au sites for electron transfer. The significant increase in k_{app} (from 15 to 5 × 10^4 times, depending on the gold amount) for the SPE/Au electrode confirms the increased electron transfer during the redox process [35]. The same effect can be observed in the CV in $[Fe(CN)_6]^{4-/3-}$ (Figure 2l), in which the peak current of the oxidation/reduction of the redox pair increased with longer electrodeposition times. This observation has important implications for the performance of electroanalytical devices. The electrochemical behavior of gold-modified electrodes was also assessed in mechanical flexion tests. Even after 50 successive manual bending cycles, no significant changes in current or potential of $[Fe(CN)_6]^{4-/3-}$ oxidation peaks were observed (deviations of 6.0% and 5.3% for current and potential, respectively, n = 3) (Figure S4).

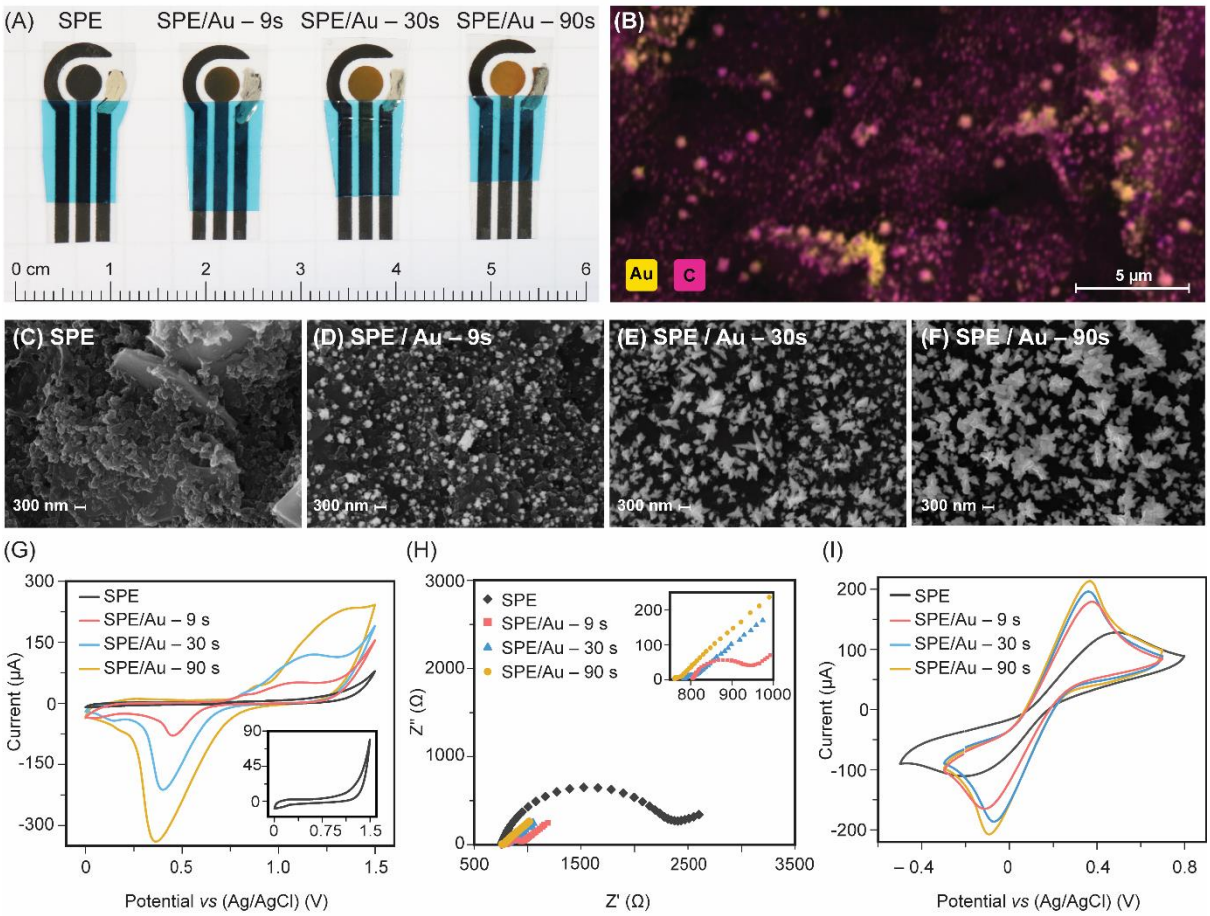

Figure 2 – (A) SPE before and after electrodeposition of gold for 9, 30, and 90 s. **(B)** Elemental mapping of an SPE after electrodeposition of gold for 9 s. Pink and yellow shades, respectively, represent carbon and gold. **(C)** bare SPE. SPE modified with gold nanostructures electrodeposited during **(D)** 9 s, **(E)** 30 s, and **(F)** 90 s. **(G)** Cyclic voltammograms in 0.1 mol L^{-1} H_2SO_4 for bare SPE (black), SPE modified with gold nanostructures electrodeposited during 9 s (red), 30 s (blue), and 90 s (yellow) at –4.0 V in a 5.0 mmol L^{-1} hydrogen tetrachloroaurate (III) solution containing 0.5 mol L^{-1} sulfuric acid. Scan rate 100 mV s^{-1}. The insert shows a zoomed view of the CV of SPE. **(H)** Nyquist plots for bare SPE (black), SPE modified with gold nanostructures electrodeposited during 9 s (red), 30 s (blue), and 90 s (yellow) in 0.1 mol L^{-1} PBS containing 4.0 mmol L^{-1} $[Fe(CN)_6]^{4-/3-}$ from 10 kHz to 10 MHz. **(I)** CVs for bare SPE (black), SPE modified with gold microstructures electrodeposited during 9 s (red), 30

s (blue), and 90 s (yellow). CV conditions: 0.1 mol L^{-1} PBS containing 4.0 mmol L^{-1} $[Fe(CN)_6]^{4-/3-}$ at a scan rate of 100 mV s^{-1}.

3.2. Assembling the immunosensor

An immunosensor was assembled with a modified SPE with a gold deposition time of 9 s and monitored through the Nyquist diagrams in Figure 3A. The use of a 9-s deposition time is justified by the increased sensitivity of these devices, as shown in the following section (3.3). The immobilization of MAA as a self-assembled monolayer (SAM) on the electrode caused R_{ct} to increase to 212.9 Ω (curve ◆, red) from 144.5 Ω for the bare electrode (curve ▼, black). A significant decrease to 76.8 Ω occurred with the immobilization with EDC/NHS, probably due to the pH used in the reaction (6.0). Antibody immobilization on the SPCE/AuNP/MAA/EDC-NHS surface increased R_{ct} slightly to 92.4 Ω. With BSA immobilization for blocking active carboxylic acids, R_{ct} increased to 259.3 Ω. The incubation of 10^{-6} mol L^{-1} antigen (SARS-CoV S protein) on the SPCE/AuNP/MAA/EDC-NHS/Ab immunosensor led to a further increase in R_{ct} to 362.4 Ω due to hindered electron mobility with the formation of the antigen-antibody complex. This complex represents an additional barrier between the electrode and $[Fe(CN)_6]^{3-/4-}$redox probes. Similar behavior was observed by Huang and co-workers, who considered the results to indicate biosensor assembling, decreasing the chances of a false positive response during impedimetric assays [36, 37]. The antibody-antigen interaction was also investigated using confocal fluorescence microscopy. The images taken before and after the interaction between MAA/EDC-NHS/Ab functionalized electrode and a fluorescein-labeled SARS-CoV S protein in Figures 3B and 3C confirm the effective biological recognition.

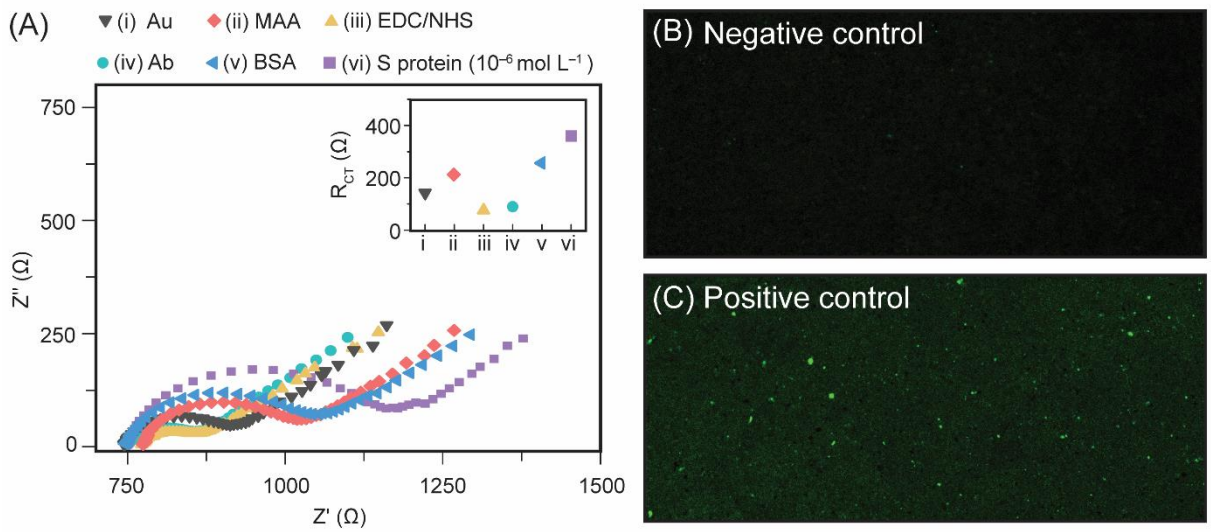

Figure 3 – (A) Nyquist plots in 0.1 mol L^{-1} phosphate buffer containing 5.0 mmol L^{-1} $[Fe(CN)_6]^{3-/4-}$ using: (i) bare SPCE/AuNP (▼ black), (ii) SPCE/AuNP/MAA (◆ red), (iii) SPCE/AuNP/MAA/EDC-NHS (▲ yellow), (iv) SPCE/AuNP/MAA/EDC-NHS/antibody (● green), (v) SPCE/AuNP/MAA/EDC-NHS/antibody/BSA (◄ blue), (vi) and SPCE/AuNP/MAA/EDC-NHS/antibody/BSA/antigen (■ purple). Conditions: 0.1 – 100,000 Hz frequency range with pulse amplitude 10 mV. Inset: equivalent circuit to fit the experimental data. The insert brings R_{ct} values (Ω) after each functionalization step calculated using $[R_s(CPE[R_{ct}Z_W])]$ as an equivalent circuit. Fluorescence images of (C) MAA/EDC-NHS/Ab functionalized electrode, and (D) functionalized electrode after detection of fluorescein-labeled protein S from SARS-CoV. Amplification 20 ×.

3.3. Analytical performance of the immunosensor

Calibration curves obtained from R_{ct} for devices constructed with three gold electrodeposition times (9, 30, and 90 s) are shown in Figure 4. All the immunosensors could differentiate SARS-CoV S protein from BSA, with R^2 and/or sensitivity values being significantly decreased for the BSA control assays. The highest sensitivity and

selectivity were observed for the immunosensor containing fewer AuNPs (9 s electrodeposition), as indicated in Figure 4D with R^2 = 0.988 and sensitivity 1.00 Ω L mol^{-1} mm^{-2}. With 9 s electrodeposition time, homogeneous spherical AuNPs are generated, thus confirming that the shape and morphology affect the electroanalytical performance [38]. For longer deposition times (30 and 90 s) – or larger gold nanostructures – the sensitivity is lower (0.258 and 0.274 Ω L mol^{-1} mm^{-2} for 30 and 90 s, respectively), with poor reproducibility (> 25%, *n* = 3) which might be due to gold leaching. Although the longer deposition time led to increased electrochemical currents (Section 3.1), electrodes with 9 s electrodeposition exhibited better analytical parameters for detecting the S protein since the resistance to charge transfer was the parameter of interest rather than the electrochemical current. Furthermore, the cost of the sensing units is decreased with less gold being deposited, and therefore the 9 s electrodeposition time was used in subsequent studies.

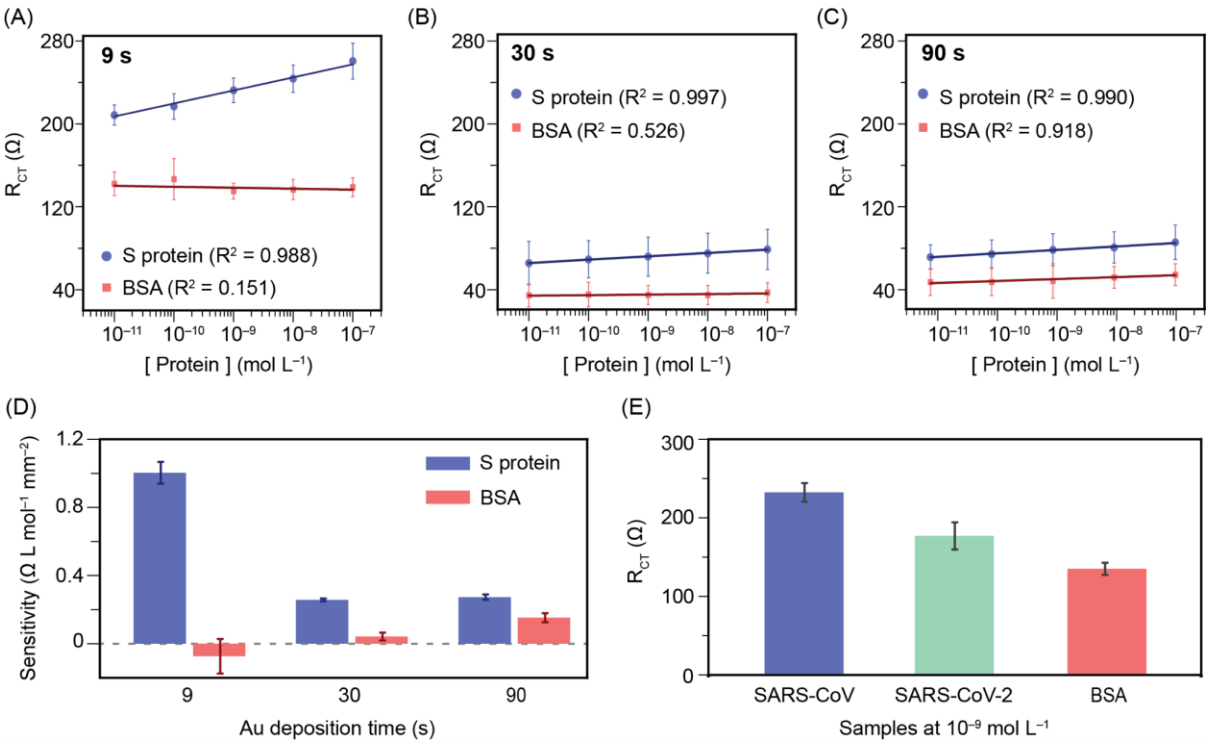

Figure 4. Calibration curves of S protein and BSA for different Au deposition times: 9 **(A)**, 30 **(B)**, and 90 s **(C)**. **(D)** Sensitivities for S protein and BSA for each Au deposition

condition. EIS conditions: 0.1 mol L^{-1} PBS containing 4.0 mmol L^{-1} $[Fe(CN)_6]^{4-/3-}$ at OCP. **(E)** R_{ct} signals from SARS-CoV, SARS-CoV-2, and BSA at 10^{-9} mol L^{-1} in PBS.

All the sensing results reported so far were obtained with SARS-CoV protein as the target analyte. We now report on the use of the same immunosensor to detect SARS-CoV-2 S protein. Figure 4E shows that SPEs modified with 9 s gold deposition time could distinguish 10^{-9} mol L^{-1} S protein from SARS-CoV, S protein from SARS-CoV-2, and BSA (control) with a statistically significant difference using the ANOVA-Tukey test ($p \leq 0.05$). To

confirm this statistical significance, we plotted the data for BSA, SARS-CoV, and SARS-CoV-2 at the same concentration of S protein (10^{-9} mol L^{-1} in PBS) using principal component analysis (PCA). Figure S5 indicates excellent distinction of the samples, with more than 94% of data explained by PCA. We emphasize that all measurements were performed with the proteins separately and at the same concentration (BSA, SARS-CoV, and SARS-CoV-2).

As expected, R_{ct} after interaction with S protein from SARS-CoV-2 had an intermediate value due to its lower interaction rate with the antibodies than the S protein from SARS-CoV. R_{ct} differs in each case which means that the immunosensor platform may be used to differentiate SARS-CoV viruses. The reason the immunosensor could be used to detect both S proteins, from SARS-CoV and SARS-CoV-2, is associated with their similar features. Indeed, SARS-CoV and SARS-CoV-2 are closely related, and their S proteins have an overall protein sequence identity of 76%. The S1 receptor-binding domain is less conserved than the S2 fusion domain (76 and 90% identity, respectively) [39]. According to the producer of anti-S protein antibodies used in this study, there is cross-reactivity with SARS-CoV-2 S protein [40].

The same was observed by Bates (2021), who measured cross-reactivity for most SARS-CoV structural protein-targeted antibodies evaluated against SARS-CoV-2 S protein [41].

The reproducibility in device fabrication was tested with three immunosensors obtained with 9 s gold deposition, which were made to interact with 10^{-9} mol L^{-1} S protein. The immunosensor reproducibility was good, with an RSD of 5.12% (*n* = 3). Although the immunosensor was designed to be disposable, the repeatability of the sensor was evaluated to ensure signal stability. This was done with ten successive measurements in a single device, and the response to 10^{-9} mol L^{-1} SARS-CoV S protein varied with a 4.51% RSD (*n* = 10). The LOD of the immunosensors was $10^{-11.5}$ mol L^{-1}. It is worth mentioning that the values used for quantifying S protein throughout this paper correspond to the total R_{ct} value from EIS measurements. Therefore, it corresponds to the biosensor itself (MAA, EDC/NHS, Antibody, BSA blocking layer) plus the analyte. We have decided to use the total R_{ct} value instead of ΔR_{ct} (before and after sample interaction) due to two main reasons. The first one is the simplification of the test for the user, requiring a single measurement. Furthermore, since using ΔR_{ct} involves two measurements rather than one, the reproducibility of the tests may be affected [31]. Indeed, the RSD% values (n=3) for R_{ct} are 5.37% before and 5.12% after sample interaction, while RSD% was 9.64% for the difference.

3.4. Application of the immunosensor in biological samples

Since saliva is a common means of transmission of infectious diseases [42], real human saliva samples were applied to evaluate the analytical performance of the immunosensor produced with 9 s gold electrodeposition. As with other coronaviruses, the spike protein is abundantly expressed during virus infection and is most effective

at inducing antibody responses in the host. Then, early diagnosis can be made by detecting antibodies against the SARS-CoV spike protein [43, 44]. SARS-CoV S protein concentrations (from 10^{-11} to 10^{-7} mol L^{-1}) were added to commercial human saliva supernatant obtained after centrifugation of the biological fluid. To assure that the changes in R_{ct} are due to antigen-antibody interactions, a control was conducted with saliva samples spiked with BSA in the same concentration range. To reduce nonspecific interactions between saliva components and the immunosensor, the latter was washed after sample incubation using PBS with the addition of a surfactant (SDS). Figure 5 shows the Nyquist plot (Figure 5A) and the calibration curves (Figure 5B) for real human saliva spiked with SARS-CoV S protein (blue) and BSA (red). The curves are similar to those where PBS was used, with R_{ct} increasing linearly (R^2 = 0.996) with the analyte addition (in log scale). As expected, a higher sensitivity was observed for S protein (5.935 Ω L mol^{-1} mm^{-2}) compared to BSA (1.725 Ω L mol^{-1} mm^{-2}). However, R_{ct} is significantly higher than in the curves with PBS, probably due to nonspecific interactions with other saliva components. The increase of R^2 (R^2 = 0.929) and sensitivity related to BSA curves corroborates this hypothesis. This behavior is probably due to the successive incubations in saliva and not due to the concentration of BSA itself. Therefore, considering a single incubation (30 min), the immunosensor can differentiate control and positive samples. It can distinguish S protein and BSA in concentrations ranging from 10^{-11} to 10^{-7} mol L^{-1} (n = 3) even in a complex environment, indicating its potential applicability in biological samples.

Last, the biosensors were tested regarding their ability to detect inactivated SARS-CoV-2 viruses in saliva samples. As expected, the measured R_{ct} was significantly increased in the presence of the virus (10^6 PFU mL^{-1}) due to interaction with the immunosensor (Figure 5C). As the typical range of positive cases of patients

infected with SARS-CoV-2 is from 10^5 to 10^7 PFU mL^{-1}, the proposed method exhibited excellent performance with potential applicability to clinical samples.

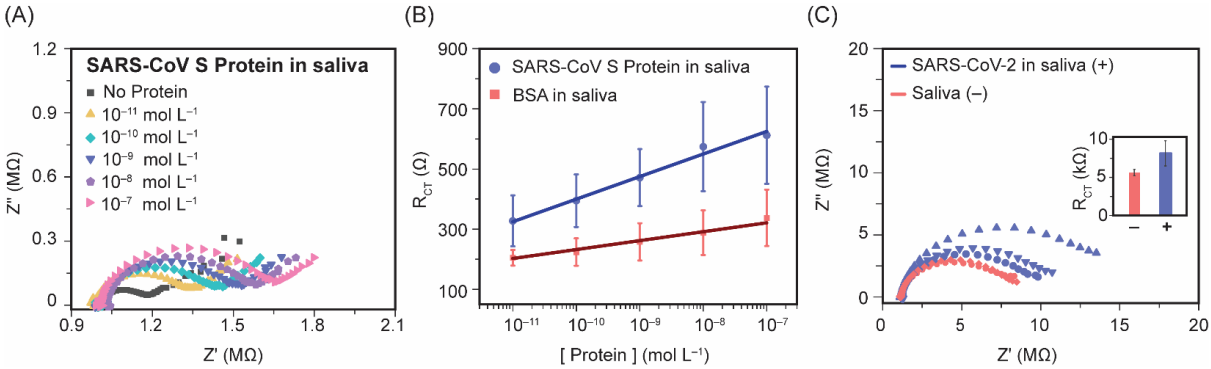

Figure 5. Application of the proposed immunosensor in biological samples. **(A)** Nyquist plots after incubation of S protein from SARS-CoV from 10^{-11} to 10^{-7} mol L^{-1} in saliva samples. **(B)** Calibration curves for S protein from SARS-CoV and BSA in saliva. **(C)** Nyquist plot for detection of inactivated SARS-CoV-2 viruses in saliva. The inset shows the R_{ct} obtained for negative (in the absence of the virus) and positive (in the presence of 10^6 PFU mL^{-1} of the virus) samples.

A list of immunosensing platforms for SARS-CoV and SARS-CoV-2 is shown in Tables S2 and S3, in the supplementary material. It is worth mentioning that none of the devices from the literature have been tested for the detection of both SARS-CoV and SARS-CoV-2, which is the case here. The immunosensor that we reported is competitive with other platforms. Even though its LOD is higher than more sophisticated immunosensors, its low cost (US$ 0.03) and potential direct applicability to biological samples represent considerable advantages. The immunosensor is also advantageous due to the ease of preparation and manipulation, as it is label-free and does not use expensive materials (graphene, carbon nanotubes) that are commonly employed in highly sensitive electrochemical sensors.

4. CONCLUSIONS

A disposable immunosensor for the sensitive determination of S proteins from SARS-CoV and SARS-CoV-2 was fabricated onto SPCEs decorated with electroformed gold nanoparticles followed by functionalization with a SAM and a layer of anti-S protein antibodies. The label-free immunosensing platform had a LOD of 3.39 pmol L^{-1} and provided quantitative results in spiked human saliva using only 10 µL in a 30 min single incubation step. The high analytical performance exhibited by the disposable immunosensor and its simple operation - with no need for signal amplification strategies - make the method an attractive alternative to identify SARS-CoV and SARS-CoV-2 in point-of-care settings. The immunosensor for S protein is competitive with other affinity electrochemical biosensors in terms of simplicity, test time, and sensitivity. The features of the simple immunosensor are promising for the deployment of mass testing in any country. To make this a reality, efforts are needed for a complete validation with a more significant number of samples and of different nature, in addition to a comparison with gold-standard techniques such as ELISA immunoassays and RT-PCR.

5. ACKNOWLEDGMENTS

The authors are grateful to São Paulo Research Foundation (FAPESP) (Grant #2018/19750-3, 2016/01919-6, 2017/05362-9, 2018/22214-6, 2020/09587-8, 2017/21097-3 and 2019/01777-5); Conselho Nacional de Desenvolvimento Científico e Tecnológico (CNPq) (Grants 164569/2020-0, 303338/2019-9 and 423952/2018-8); and Coordenação de Aperfeiçoamento de Pessoal de Nível Superior – Brasil (CAPES) (Finance Code 001; grant #3007/2014 – PROCAD; and Epidemias grant#

88887.504861/2020-00) for financial support. We would like to thank the INCTBio grants (FAPESP #2014/40867-3 and CNPq #465389/2014–7, #315824/2020-4). The authors are also greatful for Dr. Flavio Protásio Veras and Bruna Manuella Souza e Silva from Center for Research in Inflammatory Diseases (FMRP/USP) for providing inactivated virus samples.

6. REFERENCES

1. Feng W, Newbigging AM, Le C, Pang B, Peng H, Cao Y, Wu J, Abbas G, Song J, Wang D-B, Cui M, Tao J, Tyrrell DL, Zhang X-E, Zhang H, Le XC (2020) Molecular Diagnosis of COVID-19: Challenges and Research Needs. Anal Chem 92:10196–10209 . https://doi.org/10.1021/acs.analchem.0c02060
2. Hernández-Rodríguez JF, Rojas D, Escarpa A (2021) Electrochemical Sensing Directions for Next-Generation Healthcare: Trends, Challenges, and Frontiers. Anal Chem 93:167–183 . https://doi.org/10.1021/acs.analchem.0c04378
3. Raziq A, Kidakova A, Boroznjak R, Reut J, Öpik A, Syritski V (2021) Development of a portable MIP-based electrochemical sensor for detection of SARS-CoV-2 antigen. Biosens Bioelectron 178:113029 . https://doi.org/https://doi.org/10.1016/j.bios.2021.113029
4. Brazaca LC, dos Santos PL, de Oliveira PR, Rocha DP, Stefano JS, Kalinke C, Abarza Muñoz RA, Bonacin JA, Janegitz BC, Carrilho E (2021) Biosensing strategies for the electrochemical detection of viruses and viral diseases – A review. Anal Chim Acta 1159:338384 . https://doi.org/https://doi.org/10.1016/j.aca.2021.338384
5. World Health Organization (2020) Coronavirus disease 2019 (COVID-19): situation report, 52. https://apps.who.int/iris/handle/10665/331476. Accessed 12 Mar 2021

6. Hashemi SA, Golab Behbahan NG, Bahrani S, Mousavi SM, Gholami A, Ramakrishna S, Firoozsani M, Moghadami M, Lankarani KB, Omidifar N (2021) Ultra-sensitive viral glycoprotein detection NanoSystem toward accurate tracing SARS-CoV-2 in biological/non-biological media. Biosens Bioelectron 171:112731 . https://doi.org/https://doi.org/10.1016/j.bios.2020.112731
7. Ji T, Liu Z, Wang G, Guo X, Akbar khan S, Lai C, Chen H, Huang S, Xia S, Chen B, Jia H, Chen Y, Zhou Q (2020) Detection of COVID-19: A review of the current literature and future perspectives. Biosens Bioelectron 166:112455 . https://doi.org/https://doi.org/10.1016/j.bios.2020.112455
8. Fabiani L, Saroglia M, Galatà G, De Santis R, Fillo S, Luca V, Faggioni G, D'Amore N, Regalbuto E, Salvatori P, Terova G, Moscone D, Lista F, Arduini F (2021) Magnetic beads combined with carbon black-based screen-printed electrodes for COVID-19: A reliable and miniaturized electrochemical immunosensor for SARS-CoV-2 detection in saliva. Biosens Bioelectron 171:112686 . https://doi.org/https://doi.org/10.1016/j.bios.2020.112686
9. Yakoh A, Pimpitak U, Rengpipat S, Hirankarn N, Chailapakul O, Chaiyo S (2021) Paper-based electrochemical biosensor for diagnosing COVID-19: Detection of SARS-CoV-2 antibodies and antigen. Biosens Bioelectron 176:112912 . https://doi.org/https://doi.org/10.1016/j.bios.2020.112912
10. Seo G, Lee G, Kim MJ, Baek S-H, Choi M, Ku KB, Lee C-S, Jun S, Park D, Kim HG, Kim S-J, Lee J-O, Kim BT, Park EC, Kim S Il (2020) Rapid detection of COVID-19 causative virus (SARS-CoV-2) in human nasopharyngeal swab specimens using field-effect transistor-based biosensor. ACS Nano 14:5135–5142 . https://doi.org/10.1021/acsnano.0c02823
11. Alanazi K, Garcia Cruz A, Di Masi S, Voorhaar A, Ahmad OS, Cowen T, Piletska

E, Langford N, Coats TJ, Sims MR, Piletsky SA (2021) Disposable paracetamol sensor based on electroactive molecularly imprinted polymer nanoparticles for plasma monitoring. Sensors Actuators B Chem 329:129128 . https://doi.org/https://doi.org/10.1016/j.snb.2020.129128

12. Martins G, Gogola JL, Budni LH, Janegitz BC, Marcolino-Junior LH, Bergamini MF (2021) 3D-printed electrode as a new platform for electrochemical immunosensors for virus detection. Anal Chim Acta 1147:30–37 . https://doi.org/https://doi.org/10.1016/j.aca.2020.12.014
13. Cesewski E, Johnson BN (2020) Electrochemical biosensors for pathogen detection. Biosens Bioelectron 159:112214 . https://doi.org/https://doi.org/10.1016/j.bios.2020.112214
14. García-Miranda Ferrari A, Rowley-Neale SJ, Banks CE (2021) Screen-printed electrodes: Transitioning the laboratory in-to-the field. Talanta Open 3:100032 . https://doi.org/https://doi.org/10.1016/j.talo.2021.100032
15. Paschoalino WJ, Kogikoski Jr. S, Barragan JTC, Giarola JF, Cantelli L, Rabelo TM, Pessanha TM, Kubota LT (2019) Emerging Considerations for the Future Development of Electrochemical Paper-Based Analytical Devices. ChemElectroChem 6:10–30 . https://doi.org/https://doi.org/10.1002/celc.201800677
16. Du CX, Han L, Dong SL, Li LH, Wei Y (2016) A novel procedure for fabricating flexible screen-printed electrodes with improved electrochemical performance. IOP Conf Ser Mater Sci Eng 137:12060 . https://doi.org/10.1088/1757-899x/137/1/012060
17. Dungchai W, Chailapakul O, Henry CS (2009) Electrochemical detection for paper-based microfluidics. Anal Chem 81:5821–6

18. Ibáñez-Redín G, Wilson D, Gonçalves D, Oliveira ON (2018) Low-cost screen-printed electrodes based on electrochemically reduced graphene oxide-carbon black nanocomposites for dopamine, epinephrine and paracetamol detection. J Colloid Interface Sci 515:101–108 . https://doi.org/https://doi.org/10.1016/j.jcis.2017.12.085

19. Wang S, Liu N, Yang C, Liu W, Su J, Li L, Yang C, Gao Y (2015) Fully screen printed highly conductive electrodes on various flexible substrates for asymmetric supercapacitors. RSC Adv 5:85799–85805 . https://doi.org/10.1039/C5RA16724H

20. Martins TS, Bott-Neto JL, Oliveira Jr ON, Machado SAS (2021) Paper-based electrochemical sensors with reduced graphene nanoribbons for simultaneous detection of sulfamethoxazole and trimethoprim in water samples. J Electroanal Chem 882:114985 . https://doi.org/https://doi.org/10.1016/j.jelechem.2021.114985

21. Escamilla-Gómez V, Hernández-Santos D, González-García MB, Pingarrón-Carrazón JM, Costa-García A (2009) Simultaneous detection of free and total prostate specific antigen on a screen-printed electrochemical dual sensor. Biosens Bioelectron 24:2678–2683 . https://doi.org/https://doi.org/10.1016/j.bios.2009.01.043

22. Narakathu BB, Devadas MS, Reddy ASG, Eshkeiti A, Moorthi A, Fernando IR, Miller BP, Ramakrishna G, Sinn E, Joyce M, Rebros M, Rebrosova E, Mezei G, Atashbar MZ (2013) Novel fully screen printed flexible electrochemical sensor for the investigation of electron transfer between thiol functionalized viologen and gold clusters. Sensors Actuators B Chem 176:768–774 . https://doi.org/https://doi.org/10.1016/j.snb.2012.10.069

23. Qian L, Durairaj S, Prins S, Chen A (2021) Nanomaterial-based electrochemical sensors and biosensors for the detection of pharmaceutical compounds. Biosens Bioelectron 175:112836 . https://doi.org/https://doi.org/10.1016/j.bios.2020.112836

24. Kumar A, Gonçalves JM, Sukeri A, Araki K, Bertotti M (2018) Correlating surface growth of nanoporous gold with electrodeposition parameters to optimize amperometric sensing of nitrite. Sensors Actuators B Chem 263:237–247 . https://doi.org/https://doi.org/10.1016/j.snb.2018.02.125

25. Gupta P, Goyal RN, Shim Y-B (2015) Simultaneous analysis of dopamine and 5-hydroxyindoleacetic acid at nanogold modified screen printed carbon electrodes. Sensors Actuators B Chem 213:72–81 . https://doi.org/https://doi.org/10.1016/j.snb.2015.02.066

26. Satyanarayana M, Goud KY, Reddy KK, Gobi KV (2015) Biopolymer Stabilized Nanogold Particles on Carbon Nanotube Support as Sensing Platform for Electrochemical Detection of 5-Fluorouracil in-vitro. Electrochim Acta 178:608–616 . https://doi.org/https://doi.org/10.1016/j.electacta.2015.08.036

27. Cherevko S, Chung C-H (2011) Direct electrodeposition of nanoporous gold with controlled multimodal pore size distribution. Electrochem commun 13:16–19 . https://doi.org/https://doi.org/10.1016/j.elecom.2010.11.001

28. Kumar A, Furtado VL, Gonçalves JM, Bannitz-Fernandes R, Netto LES, Araki K, Bertotti M (2020) Amperometric microsensor based on nanoporous gold for ascorbic acid detection in highly acidic biological extracts. Anal Chim Acta 1095:61–70 . https://doi.org/https://doi.org/10.1016/j.aca.2019.10.022

29. Raymundo-Pereira PA, Gomes NO, Machado SAS, Oliveira ON (2019) Simultaneous, ultrasensitive detection of hydroquinone, paracetamol and

estradiol for quality control of tap water with a simple electrochemical method. J Electroanal Chem 848:113319 . https://doi.org/https://doi.org/10.1016/j.jelechem.2019.113319

30. Hernández-Saravia LP, Sukeri A, Bertotti M (2019) Fabrication of nanoporous gold-islands via hydrogen bubble template: An efficient electrocatalyst for oxygen reduction and hydrogen evolution reactions. Int J Hydrogen Energy 44:15001–15008 . https://doi.org/https://doi.org/10.1016/j.ijhydene.2019.04.186
31. Anderson DJ (1989) Determination of the lower limit of detection. Clin Chem 35:2152-2153.
32. Raymundo-Pereira PA, Shimizu FM, Coelho D, Piazzeta MHO, Gobbi AL, Machado SAS, Oliveira ON (2016) A Nanostructured Bifunctional platform for Sensing of Glucose Biomarker in Artificial Saliva: Synergy in hybrid Pt/Au surfaces. Biosens Bioelectron 86:369–376. https://doi.org/https://doi.org/10.1016/j.bios.2016.06.053
33. Carbone M, Nesticò A, Bellucci N, Micheli L, Palleschi G (2017) Enhanced performances of sensors based on screen printed electrodes modified with nanosized NiO particles. Electrochim Acta 246:580–587 . https://doi.org/https://doi.org/10.1016/j.electacta.2017.06.074
34. Karra S, Wooten M, Griffith W, Gorski W (2016) Morphology of Gold Nanoparticles and Electrocatalysis of Glucose Oxidation. Electrochim Acta 218:8–14 . https://doi.org/https://doi.org/10.1016/j.electacta.2016.09.097
35. Varodi C, Pogacean F, Coros M, Rosu M-C, Stefan-van Staden R-I, Gal E, Tudoran L-B, Pruneanu S, Mirel S (2019) Detection of 8-Hydroxy-2′-Deoxyguanosine Biomarker with a Screen-Printed Electrode Modified with Graphene. Sensors 19

36. Brazaca LC, Janegitz BC, Cancino-Bernardi J, Zucolotto V (2016) Transmembrane Protein-Based Electrochemical Biosensor for Adiponectin Hormone Quantification. ChemElectroChem 3:1006–1011 . https://doi.org/10.1002/celc.201600099

37. Huang M, Li H, He H, Zhang X, Wang S (2016) An electrochemical impedance sensor for simple and specific recognition of G–G mismatches in DNA. Anal Methods 8:7413–7419 . https://doi.org/10.1039/C6AY01705C

38. Xu J, Zhao S, Teng T, Abdalla AE, Zhu W, Xie L, Wang Y, Guo X (2020) Systematic comparison of two animal-to-human transmitted human coronaviruses: SARS-CoV-2 and SARS-CoV. Viruses 12:244

39. Jaimes JA, André NM, Chappie JS, Millet JK, Whittaker GR (2020) Phylogenetic Analysis and Structural Modeling of SARS-CoV-2 Spike Protein Reveals an Evolutionary Distinct and Proteolytically Sensitive Activation Loop. J Mol Biol 432:3309–3325 . https://doi.org/https://doi.org/10.1016/j.jmb.2020.04.009

40. Sino Biological (2021) SARS-CoV/SARS-CoV-2 Spike Antibody,Chimeric MAb. https://www.sinobiological.com/antibodies/cov-spike-40150-d006. Accessed 17 May 2021

41. Bates TA, Weinstein JB, Farley S, Leier HC, Messer WB, Tafesse FG (2021) Cross-reactivity of SARS-CoV structural protein antibodies against SARS-CoV-2. Cell Rep 34: . https://doi.org/10.1016/j.celrep.2021.108737

42. Dave PK, Rojas-Cessa R, Dong Z, Umpaichitra V (2021) Survey of Saliva Components and Virus Sensors for Prevention of COVID-19 and Infectious Diseases. Biosens. 11

43. Chang M-S, Lu Y-T, Ho S-T, Wu C-C, Wei T-Y, Chen C-J, Hsu Y-T, Chu P-C, Chen C-H, Chu J-M, Jan Y-L, Hung C-C, Fan C-C, Yang Y-C (2004) Antibody

detection of SARS-CoV spike and nucleocapsid protein. Biochem Biophys Res Commun 314:931–936. https://doi.org/https://doi.org/10.1016/j.bbrc.2003.12.195

44. Haynes LM, Miao C, Harcourt JL, Montgomery JM, Le MQ, Dryga SA, Kamrud KI, Rivers B, Babcock GJ, Oliver JB, Comer JA, Reynolds M, Uyeki TM, Bausch D, Ksiazek T, Thomas W, Alterson H, Smith J, Ambrosino DM, Anderson LJ (2007) Recombinant protein-based assays for detection of antibodies to severe acute respiratory syndrome coronavirus spike and nucleocapsid proteins. Clin Vaccine Immunol 14:331–333. https://doi.org/10.1128/CVI.00351-06

7. Manuscript Data

The data associated with this manuscript is available and has been deposited in: Canniatti Brazaca, Lais; Imamura, Amanda Hikari; Oezau Gomes, Nathalia; Bortholazzi Almeida, Mariana; Tamara Scheidt, Desirée; Raymundo-Pereira, Paulo Augusto; Novais de Oliveira Jr, Osvaldo; Campos Janegitz, Bruno; Spinola Machado, Sergio Antonio; Carrilho, Emanuel (2021), “Electrochemical immunosensors using electrodeposited gold nanostructures for detecting the S proteins from SARS-CoV and SARS-CoV-2”, Mendeley Data, V1, DOI: 10.17632/vzb9sn7cc2.1

8. Statements and declarations

The authors declare no conflict of interest.